ELSEVIER

Journal of Power Sources 113 (2003) 228–232

JOURNAL OF POWER SOURCES

www.elsevier.com/locate/jpowsour

Design aspects of the valve regulated lead/acid battery positive electrode

R.J. Ball, R. Stevens*

Department of Engineering and Applied Science, Materials Research Centre, University of Bath, Bath BA2 7AY, UK

Abstract

Experimental results obtained from the study of 12 V, 40 Ah, valve regulated lead/acid (VRLA) batteries indicated that reduction in capacity during cycling can be attributed to changes in the positive electrode. Corrosion layer (CL) growth has been identified as a key factor that can lead to a reduction in performance and eventual battery failure. In this paper, a selection of results concerned with the positive grid CL are presented. These can be used to suggest ways of improving the present positive electrode design and also to outline some of the different types of defect that form during operation. In addition, reduction in oxygen concentration through the thickness of the layer towards the grid surface was detected indicating an increase in resistivity and thus internal resistance of the cell.

Keywords: VRLA; Positive electrode; Corrosion layer

1. Introduction

Valve regulated lead/acid (VRLA) batteries have been on the market for several decades [1]. Recent advances in technology and environmental issues have resulted in an increasing demand for VRLA batteries in a range of applications, including Uninterruptible Power Supplies (UPS), Motive Power [2,3] and Starting, Lighting and Ignition (SLI) [4]. Batteries utilised in any of the above applications have a finite life due to deterioration of the various components of the battery during its operation.

Depending on the application and operational environment, battery failure can be a consequence of a range of processes involving the electrodes, electrolyte or ancillary components [5]. The most common cause of battery failure is reported to be premature capacity loss [6], which describes a reduction in performance ultimately resulting in the battery's failure. In these instances it is extremely difficult to identify the principal cause of failure. This paper describes the results obtained from the examination of cycled VRLA batteries. Details of the methods used to determine the extent of capacity loss in each individual battery cell and the contributions to this capacity loss from positive and negative electrodes are given. Results from a detailed analysis of various features of the positive electrode including current density distribution and corrosion layer (CL) growth and structure are described.

2. Experimental methods

2.1. Production of test batteries

The batteries examined in this study were all 40 Ah, 12 V monobloc units of the same design and constructed using identical materials. Positive electrodes were produced using standard grey oxide positive paste. The negative paste mix was also manufactured from grey oxide. Positive and negative grids were produced from a proprietary lead alloy. Glass microfibre separators were used, consisting of 70% coarse and 30% fine fibres. Assembled batteries were filled with electrolyte of specific gravity 1.290 at 15.5 °C prior to formation.

2.2. Cycling of test batteries

Cycling was carried out automatically using Digatron charging units. Each cycle consisted of a constant current discharge at 7.05 A to 10.2 V followed by a constant voltage recharge at 14.7 V for 16 h. This was repeated until the capacity, after charging, was less than 80% of the starting capacity.

* Corresponding author. Tel.: +44-1225-826-826; fax: +44-1225-826-098.
E-mail address: r.stevens@bath.ac.uk (R. Stevens).

0378-7753/02/$ – see front matter
PII: S0378-7753(02)00517-7

2.3. Specimen polishing

Several polishing stages were used to prepare samples. Initially specimens were flattened using 300–1200 grit size silicon carbide paper with a platen speed of 150 rpm. Water was used as a lubricant and only light pressure was applied to the sample. Texmet polishing cloth loaded with 5 and then 0.3 μm alumina suspension was used for the second stage. Finally, a texmet cloth with masterpolish was used on a Buehler Vibromet vibratory polisher, for approximately 30 min [7].

2.4. Microscopy

The polished cross-sections of corrosion layers from each battery type were examined and photographed using a Zeiss ICM405 optical microscope. CL thickness measurements were determined using Optimas image analysis software [8].

2.5. Electron probe microanalysis

A Jeol JXA-8600 superprobe was used to determine the composition of the CL. Readings were taken in a line across the CL thickness at 1 μm intervals. An initial qualitative analysis indicated that the CL consisted of lead, oxygen and sulphur. To prevent charging effects, the samples were coated with a thin layer of carbon, using an Edwards sputter coating unit. All samples and standards were coated simultaneously to reduce errors caused by adsorption of X-rays by the layer [9].

3. Results and discussion

3.1. Electrical examination of battery

A series of studies on VRLA batteries were conducted in order to identify possible causes of failure. Following failure, the state of the electrodes was determined by monitoring the voltage of each cell during a discharge/charge cycle [10]. During discharge, a reduction in the voltage of each cell was observed. For a number of batteries tested, all cells followed a very similar trend, however, in some instances a cell with greatly reduced capacity was clearly identifiable. An example is given in Fig. 1. Cell 6 shows the smallest reduction in voltage and is therefore defined as the good cell. Cell 5 shows the greatest voltage reduction and is defined as the bad cell. In order to determine if the failure was due to an individual electrode, the potentials of electrodes in the good and bad cells were measured relative to a mercury sulphate reference electrode during a discharge/charge cycle. Plots of voltage versus time are shown in Fig. 2. Results indicate that failure is due to the positive as opposed to negative electrode.

3.2. Positive electrode grid surface current density distribution

Results suggest that failure of these experimental batteries was primarily caused by degradation of the positive electrode. In order to investigate the cause of failure further, a closer examination of the positive electrode was carried out. The positive electrode consists of a current collecting grid, which also acts as a support for the porous lead dioxide positive active material (PAM). A CL is formed during battery operation between the grid and PAM. Since all current must flow through this layer, it has significant influence on battery operation. The total current is related to the total mass of PAM within the electrode and the grid surface area. Pavlov has proposed the ratio of these two parameters as a useful coefficient that can be used to compare various designs of battery electrode [11]. The variation in current density over the surface of the grid is also of importance. It is a function of the geometry of both grid and PAM. A typical example of a grid bar cross-section,

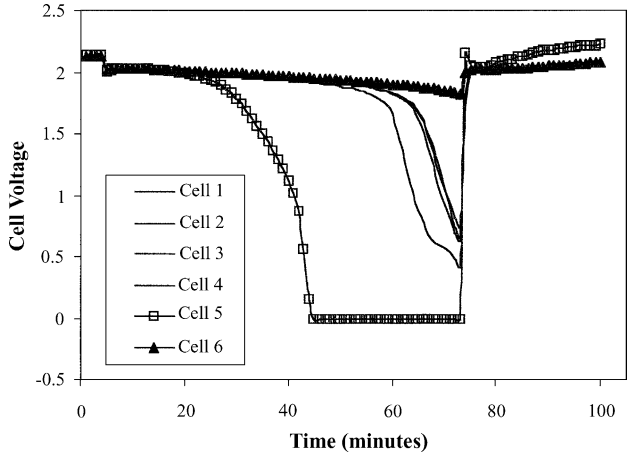

Fig. 1. Cell voltage vs. time for discharge/charge cycle after the battery had reached 80% of the starting capacity.

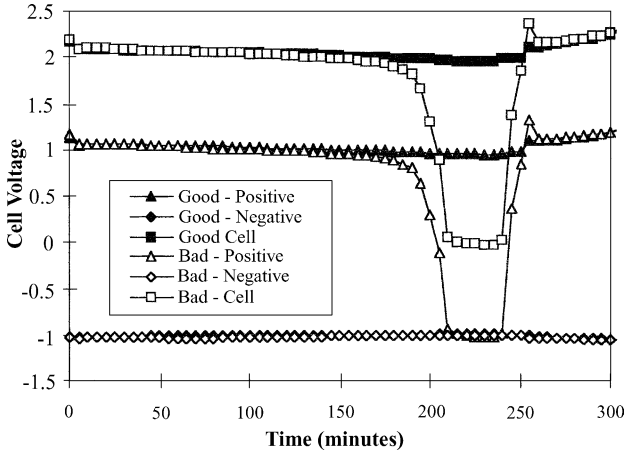

Fig. 2. Individual positive electrode, negative electrode and cell voltages during a discharge/charge cycle relative to a mercury sulphate reference electrode.

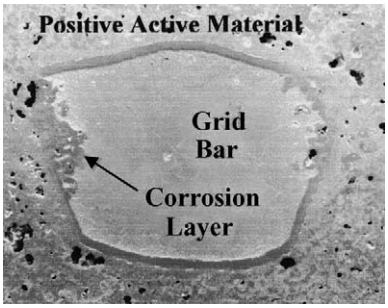

Fig. 3. Polished cross-section of grid bar showing positive active material and corrosion layer.

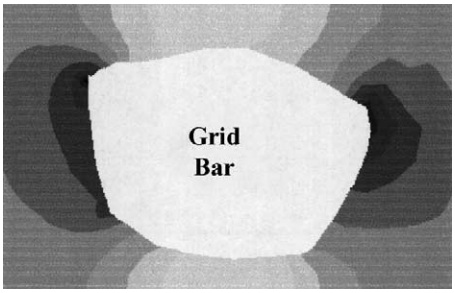

Fig. 4. Finite element model of current density distribution on surface of grid bar (darker shades of grey represent higher current densities).

prepared from the positive electrode from the bad cell, of a battery cycled approximately 90 times, is shown in Fig. 3. The grid bar is visible in the centre of the picture surrounded by the CL and PAM. A variation in CL thickness around the section is observed with the thickest sections of corrosion visible on the sides of the grid bar. Due to the uneven distribution of PAM around the circumference of the grid bar, a variation in current density is expected. This has been modelled analytically using Ansys finite element software [12]. Fig. 4 shows a contour plot illustrating the variation in current density on the surface of the grid, the darker shades of grey represent higher current densities.

A comparison of Figs. 3 and 4 suggest that CL thickness is correlated with current density. This result suggests that grid design can be improved by changing the geometry of the PAM and grid bar in order to obtain a more uniform current density distribution on the grid surface.

3.3. Corrosion layer growth during cycling

CL thickness measurements taken from a batch of identical batteries cycled to failure, which failed after varying numbers of cycles is shown in Fig. 5. Lines of best fit for the data indicate that the increase in thickness follows an exponential relationship. The increase in thickness on the bad cells is significantly larger than that for the good cells. CL growth on the positive grid occurs primarily during overcharging. A reduction in capacity of a cell results in the cell reaching a fully charged state sooner compared to the remaining cells. As the cycling regime consisted of a constant voltage recharge for a fixed length of time, this effectively increases the overcharging time and therefore CL growth.

3.4. Defects observed with the positive grid corrosion layer

CL thickening has a number of deleterious effects on the cell performance. These include increasing the resistance of the cell, through the decreased cross-sectional area of the grid bar and increased resistance of the CL. In addition to the disadvantages of the increased resistance of lead oxide compared to lead, for a current collector the CL is much more prone to the formation of defects within its structure such as cracks which can increase resistance further. Fig. 6(a) and (b) show a number of defects that form within the CL.

Fig. 6(a) shows the top left hand corner of a sectioned grid bar. The most noticeable feature is the large crack penetrating into the corner at approximately 45°. PAM in the form of a thin layer covers the internal surfaces of the crack. In addition, lower down the picture, a number of thin fissure cracks are visible. These may have been the result of

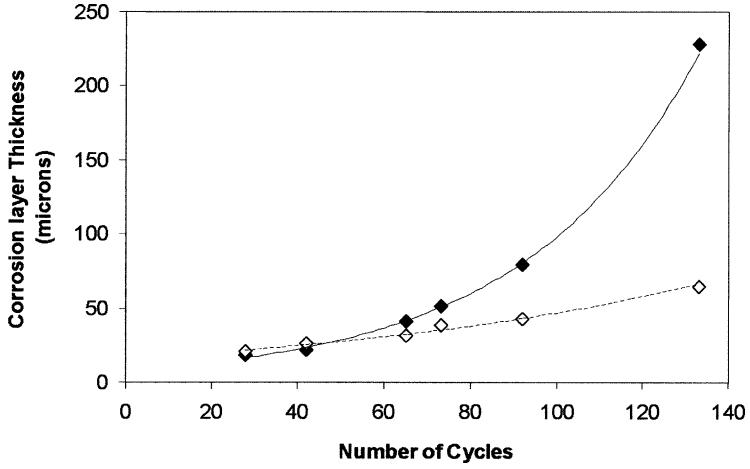

Fig. 5. Corrosion layer thickness vs. number of cycles ((◇) good cells, (◆) bad cells).

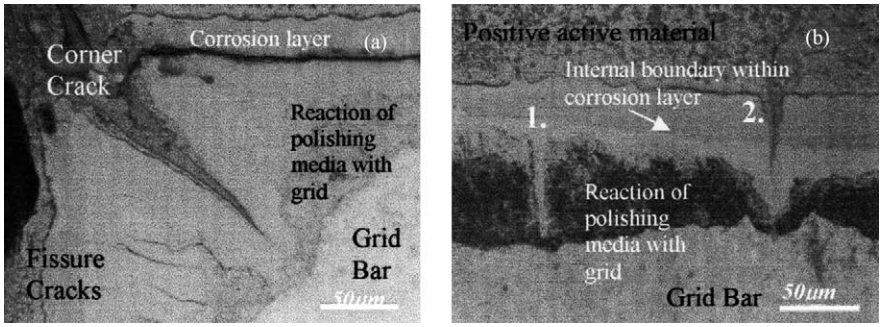

Fig. 6. Defects observed in the corrosion layer of a cycled battery. (a) The top left-hand corner of a sectioned grid bar. (b) A section of CL on the edge of the grid bar.

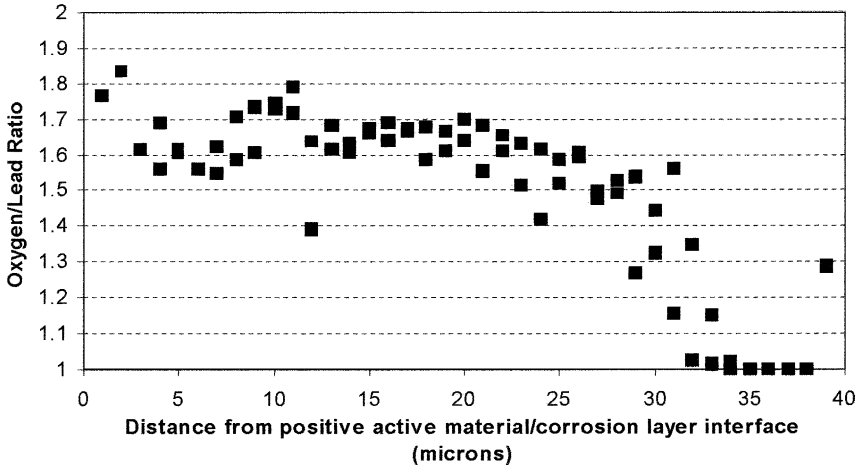

Fig. 7. Variation in oxygen concentration across the positive grid corrosion layer.

pressure acting from the evolution of gas during battery operation. A large crack is also visible in the CL on the top of the grid. This is positioned at the internal boundary of the CL where the dark and light areas of the CL meet.

Fig. 6(b) shows a section of CL on the edge of the grid bar. An internal boundary is visible in both micrographs separating a light region adjacent to the grid bar and dark region adjacent to the PAM. Reaction of the polishing media with the grid bar is responsible for the darker region at the grid/CL interface. The CL is seen to penetrate the grid in two positions: 1 and 2. Position 1 is in the form of an oxide finger growing into the grid bar. There is no feature at the CL/PAM interface to indicate the presence of the oxide finger. In comparison, a similar area where the CL is growing into the grid bar is shown at position 2. However, in this instance, a crack is visible from the CL/PAM interface to the tip of the corrosion within the grid bar. This suggests that the mechanism of growth for these two defect types is different. A close examination of defect type 2 shows the presence of some PAM within the crack. During battery cycling, the volume change associated with sulphate formation within the crack could produce a tensile opening force at the crack tip thus increasing growth. The presence of a similar mechanism in the case of defect type 2 would not be possible. An explanation could be based on the growth of oxide along a grain boundary where an increased concentration of precipitated impurities could result in a higher galvanic potential and thus enhanced corrosion. The growth of CL defects such as cracks provide pathways along which oxygen gas can diffuse. Resulting increases in oxygen concentration at the grid surface can accelerate corrosion rates above their normal levels.

3.5. Variation of oxygen concentration

The oxygen concentration within the CL and at the CL/grid interface can influence the stoichiometry and thus conductivity of the CL. A plot of oxygen/lead ratio versus distance across a CL is shown in Fig. 7. A reduction in oxygen concentration within the CL occurs with decreasing distance from the grid. This is a direct result of a reduction in the amount of oxygen able to diffuse to these areas.

The reduction in oxygen concentration adjacent to the grid surface corresponds to an increase in resistance thereby increasing the cell's internal resistance [13].

4. Conclusions

The following conclusions can be drawn from the results:

- At failure there is a variation in the capacity of each cell and it is often possible to identify a good and bad cell within a battery.
- Determination of the electrode potentials of the good and bad cells indicated that reduction in capacity could usually be attributed to changes in the positive as opposed to the negative electrode.
- Examination of polished cross-sections of positive grid bars showed an increase in CL thickness on the sides of the bar. Finite element analysis suggests that this area corresponds closely to the region of highest current density.
- The CL thickness was shown consistently to be greater on the positive electrodes in the bad cells when compared to the good cells.
- Detailed examination of the corrosion layers indicated a number of characteristic defect types. This suggests that more than one mechanism is contributing to the corrosion process.
- Oxygen concentration within the CL was shown to decrease closer to the grid wire. This lack of stoichiometry correlates with an increase in resistance.

References

[1] R.H. Newnham, Advantages and disadvantages of valve-regulated lead/acid batteries, J. Power Sources 52 (1994) 149–153.
[2] K. Takahashi, H. Yasuda, H. Hasegawa, S. Horie, K. Kanetsuki, Eight years experience with valve-regulated batteries for automotive use, J. Power Sources 53 (1995) 137–141.
[3] K. Suzuki, K. Nishida, M. Tsubota, Valve-regulated lead/acid batteries for electric vehicles: present and future, J. Power Sources 59 (1996) 171–175.
[4] T. Isoi, H. Furukawa, Valve-regulated lead/acid batteries for SLI use in Japan, J. Power Sources 59 (1996) 143–146.
[5] R. Wagner, Failure modes of valve-regulated lead/acid batteries in different applications, J. Power Sources 53 (1995) 153–162.
[6] K.K. Constanti, A.F. Hollenkamp, M.J. Koop, K. McGregor, Physical change in positive-plate material—an underrated contributor to premature capacity loss, J. Power Sources 55 (1995) 269–275.
[7] R.J. Ball, R. Evans, M. Deven, R. Stevens, Characterisation of defects observed within the positive grid corrosion layer of the valve regulated lead/acid battery, J. Power Sources 103 (2002) 207–212.
[8] OPTIMAS 6.1, Optimas UK Ltd., West Maling, Kent, UK.
[9] R.J. Ball, R. Kurian, R. Evans, R. Stevens, Influence of positive active materials type and grid alloy on corrosion layer structure and composition in the valve regulated lead/acid battery, J. Power Sources 111 (1) (2002) 23–38.
[10] R.J. Ball, R. Kurian, R. Evans, R. Stevens, Failure mechanisms in valve regulated lead/acid batteries for cyclic applications, J. Power Sources 109 (1) (2002) 189–202.
[11] D. Pavlov, A theory of the grid/positive active-mass (PAM) interface and possible methods to improve PAM utilisation and cycle life of lead/acid batteries, J. Power Sources 53 (1995) 9–21.
[12] R.J. Ball, R. Evans, R. Stevens, Finite element (FE) modelling of current density on the valve regulated lead/acid battery positive grid, J. Power Sources 103 (2002) 213–222.
[13] F. Lappe, Some physical properties of sputtered PbO_2 films, J. Phys. Chem. Solids 23 (1962) 1563–1572.